

Influence of space charge on the scale-up of multiplexed electrospays

Weiwei Deng, Alessandro Gomez*

Department of Mechanical Engineering, Yale University, New Haven, CT 06520-8286, USA

Received 22 June 2007; received in revised form 21 August 2007; accepted 22 August 2007

Abstract

The effect of the space charge of the homopolarly charged droplets in a system of multiplexed electrospays is investigated. The system consists of a microfabricated liquid distributor with multiple electrospay sources held at a high voltage, a nearby extractor electrode plate held at an intermediate voltage, and a grounded electrode further downstream. The system is very compact, with a spatial density as large as 250 sources/cm². Experimentally, we observed that the system performance was limited by the occurrence of path reversal of the satellite droplets, accumulating on the extractor electrode, flooding it and ultimately causing the electrospay to cease operation. To prevent this phenomenon, hereafter referred to as satellite trapping, and “sweep” the satellites downstream, the driving field between the extractor electrode and the ground must be increased. The system behavior was modeled by a simple line-of-charge approximation, which was validated by a more detailed Lagrangian model and by experiments on an individual electrospay. Subsequently, the line-of-charge model was extended to the multiplexed system yielding a satisfactory comparison between the computed minimum driving field that is necessary to prevent satellite path reversal and experimental values. Additional analytical approximations of the multilines-of-charge model yielded a scaling law showing the dependence of the space charge on: (i) the primary droplet residence time, (ii) the current emitted per unit area, and (iii) a dimensionless parameter, α , that is the ratio of the distance between the extractor electrode and the ground electrode to the distance between neighboring nozzles. As a result, guidelines for the design of multiplexed electrospays are established on a fundamental basis, without the need for costly and empirical microfabrication prototyping.

© 2007 Elsevier Ltd. All rights reserved.

Keywords: Electrospay; Microfabrication; Multiplex; Space charge

1. Introduction

The electrospay of conducting liquids operated in the cone-jet mode (Cloupeau & Prunet-Foch, 1989) has the unmatched capability of producing monodisperse particles with relative ease, especially in the nanometric scale range. Since the electrospay exhibits a monotonic dependence of droplet size on flow rate (e.g., Chen & Pui, 1997; Rosell-Llompарт & Fernandez de la Mora, 1994; Tang & Gomez, 1994), if small droplets are desired as in applications such as nanoparticle synthesis, the mass flow rate is invariably minuscule (Gomez, Bingham, De Juan, & Tang, 1998). The low throughput of the electrospay is a particularly severe drawback that has hampered its widespread application

* Corresponding author. Tel.: +1 203 432 4384; fax: +1 203 432 7654.

E-mail address: Alessandro.Gomez@yale.edu (A. Gomez).

Nomenclature

A	average area per nozzle, $A = \sqrt{3}/2P^2$
C_D	drag coefficient of the droplet
C_∞	constant coefficient: $C_\infty = 3\sqrt{3}/2\pi\epsilon_0 = 0.827/\epsilon_0$
C_s	constant coefficient: $C_s = 0.5/\epsilon_0$
D_o	diameter of the orifice on the extractor
\bar{D}	droplet size averaged over all jets: $\bar{D} = \sum \bar{D}_i/N$
\bar{D}_i	average droplet diameter for jet i
d	primary droplet mean diameter
d_i	diameter of the i th droplet
E_∞	axial component of total space charge field of an infinitely large system
E_j	electric field in the jet forming region
E_d	driving field in the spray region
\vec{E}_e	external electric field
E_r	radial component of the space charge field
E_{ref}	reference field: $E_{\text{ref}} = 3\lambda/(\pi\epsilon_0 P)$
E_{sum}	axial component of total space charge field of a system with n spray “rings”
E_z	axial component of the space charge field
E_{z0}	minimum driving field to eliminate the “satellite trapping” in a single spray
E_{zn}	axial component of space charge field caused by the n th spray ring
\vec{e}_i	velocity unit vector of i th droplet
\vec{F}_{image}	image force
I	current carried by a single electrospray
K	liquid conductivity (S/m)
n	number of concentric “rings” of multiplexed sprays
N_d	number of droplets in the computational domain
N	number of nozzles on the liquid distributor chip
OD	outer diameter of the nozzle
P	distance between two neighboring nozzles
Q	liquid volume flow rate per nozzle
q	total charge enclosed in the control volume
q_i	charge of the i th droplet
RSD	relative standard derivation: $\text{RSD} = \frac{1}{\bar{D}} \sqrt{\sum_{i=1}^N (\bar{D}_i - \bar{D})^2 / (N - 1)}$
r	radial displacement of the droplet
\vec{r}_{ij}	displacement vector of the i th and the j th droplets
t_B	jet break up time: $t_B = \pi d^3 / 6Q$
\vec{u}_i	velocity of the i th droplet
v_g	gaseous (air) velocity
v_z	axial velocity of the primary droplets
z	axial displacement of the droplet
z_0	distance between the extractor electrode and the collector electrode
Δt	time interval
α	aspect ratio of the electrode system ($\alpha = z_0/P$)
β	dimensionless parameter in determining the boundary layer
ϵ	dielectric constant of the liquid
ϵ_0	permittivity in vacuum
δ	thickness of the boundary layer
λ	line-of-charge density (C/m)

ν	kinematic viscosity of the ambient air
ρ_g	mass density of the ambient air
ρ_l	mass density of the droplet
ρ_s	volume charge density
τ	charge relaxation time: $\tau = \epsilon\epsilon_0/K$

Subscript

prim	primary droplet
sat	satellite droplet
i	i th droplet

to areas other than electrospray ionization mass spectroscopy (ESI-MS) (Fenn, Mann, Meng, Wong, & Whitehouse, 1989). Intuitively, multiplexing the spray source is a possible remedy to overcome this drawback and may open the door to high value-added applications such as the synthesis of nanoparticles for a variety of uses.

We recently reported on the successful development of a microfabricated system of multiplexed electrosprays with a packing density of 250 sources/cm² (Deng, Klemic, Li, Reed, & Gomez, 2006). We demonstrated an increase in throughput by up to two orders of magnitude without losing the capability of generating monodisperse droplets. One crucial factor making high density multiplexing possible is a careful selection of the electrode configuration, which entails an extractor electrode mounted at a distance from the spray sources that is comparable to the distance between sources. The extractor electrode has the dual function of limiting electrostatic interference between neighboring sources and shielding Taylor cones electrostatically from the spray cloud. This system was successfully applied in a high power-density liquid fuel micro-combustor (Deng, Klemic, Li, Reed, & Gomez, 2007).

This system, along with similar efforts in multiplexing (Bocanegra, Galán, Márquez, Loscertales, & Barrero, 2006; Tang, Lin, Matson, Kim, & Smith, 2001; Velásquez-García, Akinwande, & Martínez-Sánchez, 2006), will inevitably face difficulties in operating reliably as packing density, liquid conductivity, and flow rate increase. Two obstacles could arise: first the space charge from the parallel sprays may destabilize the cone-jets anchoring the electrosprays and, in turn, affect the spray atomization; second, the droplets may reverse their path and accumulate on the extractor plate, bridging electrodes and eventually shorting out the device.

The space charge for a single needle-to-plate electrospray source has been investigated for its influence on the angle of the Taylor's cone (Fernández de la Mora, 1992). A study related to the present one is the field-reduction work on a colloid thruster array, where the Child–Langmuir's law was recovered to evaluate the current density (Lozano, 2003). However, a clear and detailed picture of the complications ensuing from the multiplexed electrosprays is still lacking.

We report here a systematic study on space charge effect, including both a computational component and an experimental one. The study sheds light on the space charge field and on the mechanism of the droplet path reversal that is ultimately the limiting factor to an increase in the multiplexing density (number of sprays per unit area). We conclude with a scaling law and a design criterion to estimate the multiplexing limit as a function of critical variables, such as the primary droplet residence time and the current emitted per unit area.

2. Experimental approach

The key component of the experimental system is the multiplexed electrospray distributor chip. The device was microfabricated in the U.S. Army Research Laboratory (ARL) using Deep Reactive Ion Etch (DRIE) of silicon wafers. Uniform nozzles with an outer diameter of 210 μm , interspaced at 675 μm , and protruding 450 μm were patterned. The detailed fabrication, testing, and fundamentals of the first-generation distributor were documented in Deng et al. (2006). In the current nozzle geometry, the inner diameter was decreased from 120 to 60 μm to ensure uniformity of droplet size in all sprays. In fact, in such a case, viscous drag in the nozzle is the dominant force controlling the flow rate through each nozzle, non-uniformities in the electric field are of secondary importance and the flow rate is uniformly distributed. Consequently, the droplet size, that is monotonically dependent on flow rate, does not vary from spray to

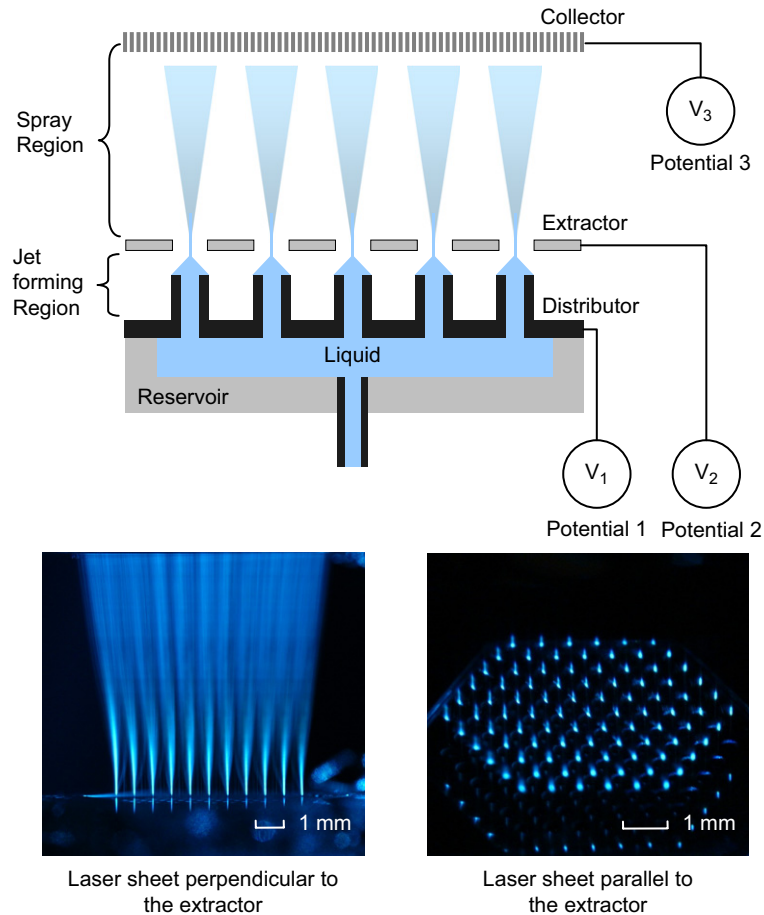


Fig. 1. Electrode configuration and spray visualization.

spray. Indeed, the relative standard deviation $RSD = \frac{1}{\bar{D}} \sqrt{\frac{\sum_{i=1}^N (\bar{D}_i - \bar{D})^2}{N-1}}$ was less than 3%, where \bar{D}_i is the average droplet diameter for jet i , and $\bar{D} = \sum \bar{D}_i / N$ is the droplet size averaged over all jets. Arrays with 1, 7, 19, 61, 91, or 331 nozzles were tested, and all arrays had the same initial number density of 250 sources/cm², except when a portion of the nozzles was deliberately blocked to study the effect of lower number density.

Fig. 1 shows a typical testing arrangement, which consisted of three electrodes: the distributor electrode that was mounted on a liquid reservoir, the extractor electrode that was positioned 400 μm above the distributor with a Pyrex spacer/insulator sandwiched between the two, and a flat metal collector electrode 10 mm away from the extractor. The region between the liquid distributor chip and the extractor is therefore named the jet forming region, and the space between the extractor and the collector is defined as the spray region. The electrodes were maintained at different potentials to achieve the desired electric fields. A strong field, E_j , was established in the jet forming region to anchor the cone-jets, and a driving field, E_d , was established in the spray region to guide the charged droplets toward the collector. The system was operated in air at atmospheric pressure with driving fields less than 10^6 V/m. When even more intensive electric fields were required to test limits of the system behavior, the air was replaced with CO₂ to reduce the risk of corona discharges in view of the higher breakdown voltage of that gas. No charge neutralization mechanism was introduced in the experiment.

The current was measured by connecting the virtual ground to a voltmeter with known input impedance. Visual observation of the mode of operation was made possible by a laser beam, which was first expanded and then focused by a 300 mm cylindrical lens into a laser sheet. The orientation of the laser sheet could be either parallel or perpendicular to the distributor surface. For the parallel orientation, the scattering of charged droplets in each spray resulted in the

visualization of individual spray cross-sections appearing as small circular spots, while the perpendicular orientation allowed for the visualization of spray plumes. Images in both orientations are shown in Fig. 1.

We tested two liquids with different conductivities: pure ethanol, with conductivity measured at 1.3×10^{-5} S/m and ethanol doped with 5 ppm by weight of an ionic liquid, 1-ethyl-3-methylimidazolium ethylsulfate, with conductivity $K = 1.0 \times 10^{-4}$ S/m. The liquid was pumped continuously into the reservoir by a syringe pump with different syringe sizes to ensure that the plunger would be displaced at a reproducible and accurate speed. Droplet sizes were measured by an optical fiber Phase Doppler Particle Analyzer (PDPA) (TSI) capable of measuring simultaneously the droplet size and two velocity components from the scattering of a frequency-modulated argon ion laser beam (Coherent).

3. Modeling approach

The single electro spray was modeled with a Lagrangian single-droplet tracking of a dilute two-phase flow (Ganan-Calvo, Lasheras, Davila, & Barrero, 1994; Wilhelm, Mädler, & Pratsinis, 2003). The Lagrangian model predicts the electro spray behavior accurately, but it is impractical to simulate hundreds or thousands of electro spray sources simultaneously, because the CPU time scales with N_d^2 , where N_d is the number of droplets in the computational domain. As an alternative, we pursued a line-of-charge model which could be easily scaled up, without compromising the ability of describing crucial space charge features. The line-of-charge model was validated by comparison with both the Lagrangian model and some targeted experiments.

3.1. Approximation of the space charge field by a line-of-charge model

As shown in Fig. 1, a typical plume in the multiplexed electro spray has an aspect ratio, $\alpha = z_0/P$, of order 10, where z_0 is the distance between the extractor electrode and the collector electrode, and P is the distance between two neighboring nozzles. The slenderness of the spray suggests that, in terms of induced electric field, the spray may be approximated as a line-of-charge. Accordingly, we made the following assumptions:

- (1) the spray is a continuous line-of-charge, that is perpendicular to the extractor surface, starting from the extractor at $z = 0$ and ending at the collector at $z = z_0$;
- (2) the charge density (charge per unit length) $\lambda = I/v_z$ is uniform, where I is the current carried by a single electro spray, and v_z is the initial jet velocity; and
- (3) the line-of-charge introduces one image charge on the opposite side of each of the two conducting surfaces and perpendicular to them, each image charge having length z_0 and charge density $-\lambda$.

The second assumption requires that the velocity of the primary droplet is nearly a constant. Indeed, Fig. 2 shows that the velocity of the primary droplets exhibits a small (less than 10%) variation along axial direction. This trend is typical. Moreover, as we will show later, the “critical zone” of particular interest is within approximately the first millimeter above the extractor, within which the constant velocity assumption is certainly justified even if the primary droplets were accelerated outside the critical zone by an intense driving field, unlike the current experiment.

In order to evaluate the space charge field at the position (r, z) , we combine the effect of the three segments (the line-of-charge and its two images):

$$E_r = \frac{\lambda}{4\pi\epsilon_0 r} \left[\frac{2z}{\sqrt{r^2 + z^2}} + \frac{2(z_0 - z)}{\sqrt{r^2 + (z_0 - z)^2}} - \frac{z_0 + z}{\sqrt{r^2 + (z_0 + z)^2}} - \frac{2z_0 - z}{\sqrt{r^2 + (2z_0 - z)^2}} \right], \quad (1)$$

$$E_z = \frac{\lambda}{4\pi\epsilon_0} \left[\frac{2}{\sqrt{r^2 + (z_0 - z)^2}} - \frac{2}{\sqrt{r^2 + z^2}} + \frac{1}{\sqrt{r^2 + (z_0 + z)^2}} - \frac{1}{\sqrt{r^2 + (2z_0 - z)^2}} \right]. \quad (2)$$

At $r \ll z$ and $r \ll (z_0 - z)$, i.e., for positions relatively distant from the edge, Eq. (1) becomes

$$E_r \simeq \frac{\lambda}{2\pi\epsilon_0 r}. \quad (3)$$

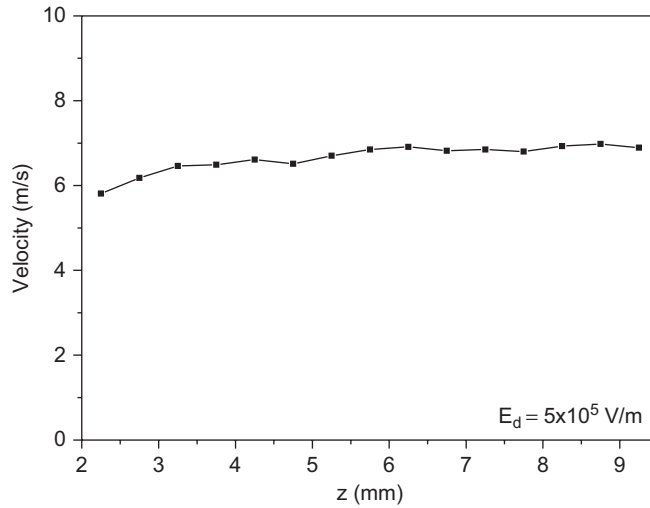


Fig. 2. Droplet velocity profile along the axial direction for a typical spray.

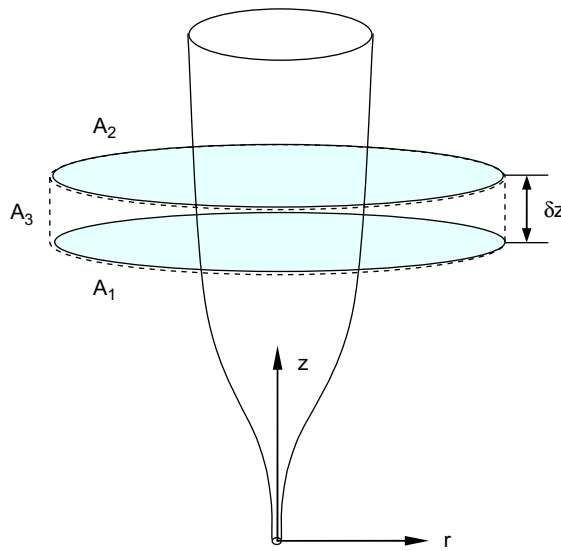


Fig. 3. Spray plume control volume.

Eq. (3) can be also verified by the following analysis. Consider the spray plume and the cylindrical “pill box” control volume shown in Fig. 3. A_1 , A_2 , and A_3 are the bottom surface, the top one, and the side one, respectively. Applying Gauss law to this control volume, one obtains:

$$q/\epsilon_0 = \oint \vec{E} \cdot \hat{n} \, dA = \int_{A_1} \vec{E}_1 \cdot \hat{n}_1 \, dA + \int_{A_2} \vec{E}_2 \cdot \hat{n}_2 \, dA + \int_{A_3} \vec{E}_3 \cdot \hat{n}_3 \, dA, \tag{4}$$

where q is the total charge enclosed by the control volume, i.e. the volume integral of the space charge density ρ_s , that is,

$$q = \int_V \rho_s \, dV = \int_z \left(\int_A \rho_s \, dA \right) dz = \int_z \lambda \, dz = \lambda \delta z. \tag{5}$$

As the height of the pill box shrinks and approaches zero, $A_1 \rightarrow A_2$, $E_1 \rightarrow E_2$, the first two terms of the RHS of Eq. (4) become

$$\lim_{\delta z \rightarrow 0} \int_{A1} (\vec{E}_1 - \vec{E}_2) \cdot \hat{n}_1 dA = 0. \quad (6)$$

The third term on the RHS of Eq. (4) is

$$\int_{A3} \vec{E}_3 \cdot \hat{n}_3 dA = E_r (2\pi r \delta z). \quad (7)$$

Combining Eqs. (4)–(7), we recover Eq. (3). We point out that the line-of-charge model applies effectively only in the domain *outside* the primary spray plume, since the control volume must enclose all the primary droplets and the field is singular at the location of the line. Fortunately, the region outside the primary spray is of greatest interest, because it is where the satellite droplets are segregated by initial electrostatic/inertial effects.

The analytical expression of E_z and E_r of the line-of-charge simplifies the modeling dramatically. An example of its convenience is the computation of the plume shape, as determined by the location of the outermost primary droplets. The equation of motion for these droplets is

$$\begin{aligned} d^2z/dt^2 &= dv_z/dt = (E_z + E_d)(q_{\text{prim}}/m_{\text{prim}}) + F_{z,\text{drag}}/m_{\text{prim}}, \\ d^2r/dt^2 &= dv_r/dt = E_r(q_{\text{prim}}/m_{\text{prim}}) + F_{r,\text{drag}}/m_{\text{prim}}. \end{aligned} \quad (8)$$

Eq. (8) describes the trajectory of the outermost primary droplet, or the plume shape. Since the satellite droplet is always outside the primary droplet spray, its motion could be modeled by the line-of-charge approximation as well:

$$\begin{aligned} d^2z/dt^2 &= dv_z/dt = (E_z + E_d)(q_{\text{sat}}/m_{\text{sat}}) + F_{z,\text{drag}}/m_{\text{sat}}, \\ d^2r/dt^2 &= dv_r/dt = E_r(q_{\text{sat}}/m_{\text{sat}}) + F_{r,\text{drag}}/m_{\text{sat}}. \end{aligned} \quad (9)$$

3.2. Lagrangian model

Following Ganan-Calvo et al. (1994) and Wilhelm et al. (2003), we developed a Lagrangian code to validate the line-of-charge model for the single spray case. The Lagrangian code tracks each droplet in a dilute two-phase flow. The force balance on the i th droplet is

$$\frac{\pi}{6} d_i^3 \rho_l \frac{d\vec{u}_i}{dt} = C_D \frac{\pi}{8} \rho_g d_i^2 (u_i - v_g)^2 \vec{e}_i + q_i \vec{E}_e + \frac{1}{4\pi\epsilon_0} \sum_{ij, i \neq j} \frac{q_i q_j}{r_{ij}^3} \vec{r}_{ij} + \vec{F}_{\text{image}}. \quad (10)$$

The RHS terms account for the drag force by the surrounding gas, the force on the droplets by the external electric field, the mutual electric force between charged droplets, and the electric force between the i th droplet and the induced charge on conductive substrates (image force), respectively. In the computation of the image force, we only considered the image charges induced by the charged droplets on the extractor and collector surfaces, both of which are treated as large planes.

The space charge field is determined from the spatial distribution of each droplet, whose motion is governed by Eq. (10). Thus, we first collected all the information needed in Eq. (10). The actual scenario that we simulated was that of a single ethanol electrospray operating in the cone-jet mode at the volume flow rate of 0.6 cc/h. We assumed that the spray only consisted of two groups of monodispersed droplets, primary ones and satellites, consistently with previous findings in similar liquids (Tang & Gomez, 1994). The initial droplet velocity and diameters of primary and satellite droplets were directly measured by PDDA. For the ethanol electrospray to be modeled, the charge relaxation time $\tau = \epsilon\epsilon_0/K$ is one order of magnitude larger than the jet breakup time $t_B = \pi d^3/6Q$, where ϵ is the dielectric constant of the liquid, ϵ_0 is the electrical permittivity in vacuum, d is the primary droplet mean diameter, and Q is the flow rate. Consequently, the charge remains approximately frozen during the jet breakup, and the volumetric charge density can be considered constant for all droplets (De Juan & Fernández de la Mora, 1997). The mass and the charge of droplets were calculated from the current, the volume flow rate, and the droplet diameters.

The gaseous entrainment introduced by the jet may be important because the axial gas velocity changes significantly across the boundary layer, which could play a role in the drag evaluation. Furthermore, the satellite droplets, the behavior of which is particularly critical as will be shown below, are even more likely to be affected by the viscous force because of their small Reynolds numbers. Therefore, a boundary layer sub-model based on the momentum integral of an assumed velocity profile was adopted to estimate the entrained gas velocity field v_g . The early stage of the spray was treated as a continuous cylindrical surface, and the boundary layer started from the cone apex from where the jet emitted. As discussed in Sakiadis (1961) and references therein, the success of the integral momentum equation in determining the boundary-layer behavior depends heavily on how well the assumed velocity profile represents the conditions existing near the surface. It has been shown that the logarithmic type velocity profile is appropriate for a cylindrical surface of finite length. For continuous cylindrical surfaces, the appropriate velocity profile should be also logarithmic. Thus the following dimensionless boundary layer thickness and velocity profile were imposed (Sakiadis, 1961):

$$\frac{\delta}{r_{\text{jet}}} = e^{\beta} - 1,$$

$$\frac{v_g}{v_{\text{jet}}} = \left\{ 1 - \frac{1}{\beta} \ln \left(\frac{r}{r_{\text{jet}}} \right) \right\}, \quad (11)$$

where β is a function of z determined by the integral equation:

$$\frac{4vz}{r_{\text{jet}}^2} = 2 \int_{\beta=0}^{\beta} \left(\frac{\beta e^{2\beta} - e^{2\beta}}{\beta^2} + \frac{1}{\beta} + \frac{1}{\beta^2} \right) d\beta. \quad (12)$$

E_e was computed by a COMSOL Multiphysics (COMSOL, 2007) model which contains the geometry information of the nozzle, jet, extractor, and collector. The result was then exported to the Lagrangian code.

Eq. (10) was solved by a fourth order Predictor–Corrector algorithm (Frenkel & Smit, 2002) which yielded an optimal compromise between stability and accuracy for a given time step. The time interval Δt was chosen as the time elapsed between generating a primary droplet and a satellite one, which is of the order of 1.5 μs . The computational domain was cylindrical in the spray region, measuring 10 mm in height and 10 mm in diameter. The two parallel boundary surfaces were extractor and collector electrodes. Both primary and satellite droplets with small random radial perturbations of the order of the primary droplet diameter entered into the domain at the center of the extractor. Once the steady state was reached, the space charge field (E_r , E_z) could be calculated from the second to the last term in Eq. (10), based on the individual droplet position in each snapshot. Because of axial symmetry, we only computed the space charge field in the radial plane containing the axis. The grid for calculating the space charge field was 50 (radial) by 50 (axial) and the cell size is 0.1 mm \times 0.2 mm. Smoother field could be achieved by averaging the results from 50 snapshots.

4. Results and discussion

4.1. Space charge feedback

First we examined whether the space charge penetrates the orifice of the extractor electrode, weakens the field near the cone and eventually destabilizes the electrospray. If this were to occur, the space charge might limit the range of flow rates and consequently of droplet sizes within which stable operation can be achieved. This effect was evaluated by computing the relative field variation near the nozzle with and without space charge. We assumed that a hemispherical liquid drop was positioned at the nozzle tip, although the selection of the meniscus geometry is not critical since we will be performing a relative comparison. The drop and the nozzle were equipotential. A driving field in the same direction as the space charge field, that is, from the collector to the extractor, and of the same intensity as the breakdown limit of air (3×10^6 V/m) was imposed in the spray region to provide an upper limit to the space charge field, then the field at the top of the drop was compared with that in the absence of the driving field. The relative variation of the local field due to the imposed “pseudo space-charge” was found to be less than 1.4% for $D_o/H = 1.14$, where D_o is the diameter of the orifice on the extractor and H the spacer thickness. When $D_o/H = 0.57$, the relative variation was only 0.1%. In this work, as more generally, in practical realizations of the extractor, D_o/H was less than unity for all devices. Therefore the space charge feedback is anticipated to be very modest.

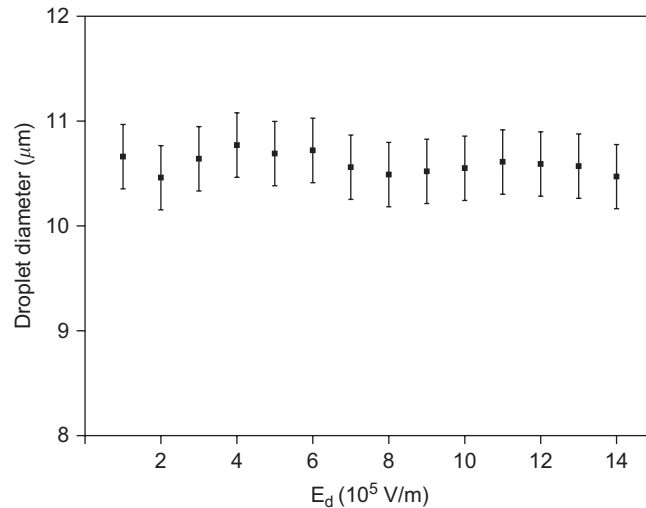


Fig. 4. Effect of driving electric field between extractor and collector on droplet size.

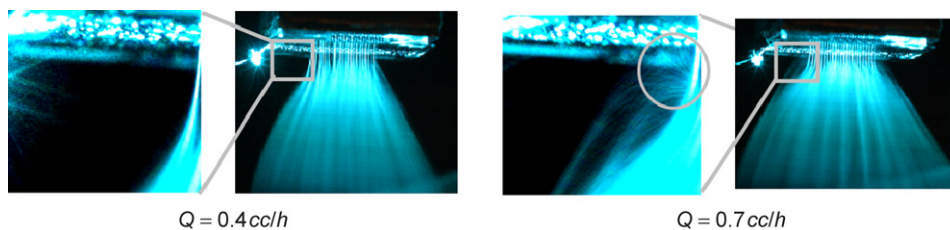


Fig. 5. Photographic evidence of droplet path-reversal as the average flow rate per nozzle increases.

We also performed experiments to verify the results of the simulation. The goal was to monitor the droplet size as E_d applied between the extractor and the collector was varied. Results are shown in Fig. 4. E_d ranged in value from 10^5 V/m to as much as 1.4×10^6 V/m, without any noticeable change in droplet size. We conclude that the extractor is a good electrostatic shield and space charge in the spray region has a negligible effect on the jet forming region.

4.2. Satellite trapping

Fig. 5 shows pictures taken from the system described earlier with the laser sheet perpendicular to the extractor plate at two flow rates. The zoomed-in image on the left, at an average flow rate of 0.4 cc/h per nozzle, suggests that all the droplets traveled in the same direction toward the collector. But when the average flow rate was increased to 0.7 cc/h, some droplets reversed their path and flew back toward the extractor, as shown in the middle-right picture (circled area) in Fig. 5.

The path reversal should appear first for droplets with smaller diameters, i.e. the satellites, since the deceleration caused by the drag is larger for smaller droplets. Experimental confirmation was found in the diameter–velocity correlation measurement shown in Fig. 6. In this experiment, the PDBA probe volume was first placed on the spray axis, and then the probe volume was moved along the radial direction into the shroud of the spray. The positive direction of the velocity is defined as from the extractor to the collector. When the driving field between the extractor to the collector was decreased to a certain level (below 7.5×10^4 V/m for ethanol running at 0.6 cc/h), the PDBA measured negative velocities in the shroud, attesting to the path reversal. Two distinct clusters of data can be identified in Fig. 6 with the sizes of the droplets with negative velocities at about $\frac{1}{3}$ to $\frac{1}{2}$ of that of the other droplets moving in the opposite direction. This result confirms that the satellites start to reverse their path. This phenomenon is heretofore referred to as *satellites trapping*, whereas the primary droplets that carry the majority of the spray mass and charge persist in

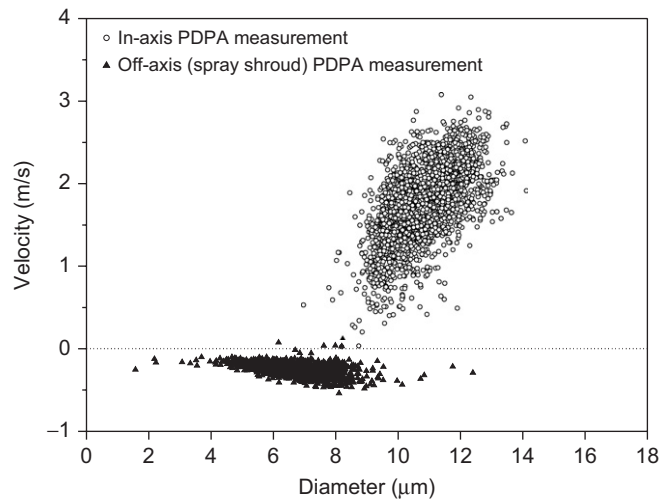


Fig. 6. Velocity and diameter correlation for an individual electrospray.

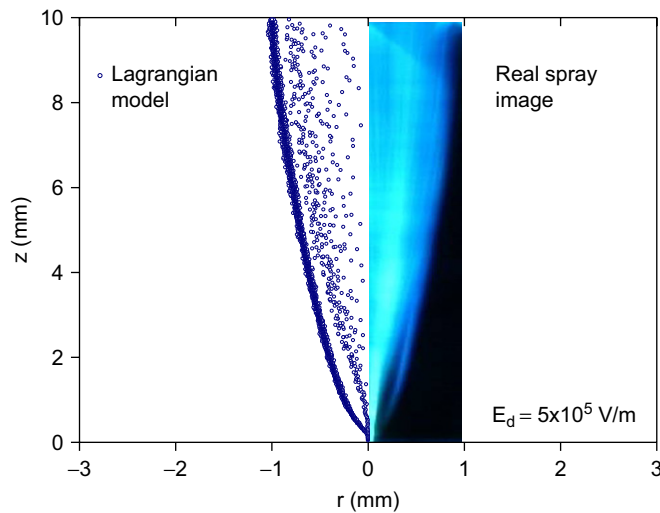


Fig. 7. Comparison between the computed spray plume (left), with each symbol representing a droplet position, and the photograph of the spray (right).

their motion toward the collector electrode. This conclusion typically applies to electrospray breakup resulting in two distinct droplet sizes, even though the difference in size may vary on the basis of the physical properties of the dispersed liquid (Li, Tu, & Ray, 2005). To quantify the phenomenon of satellite trapping, we shall rely on a model of the electric field as illustrated in the subsequent sections.

4.3. Model verification: space charge field of a single electrospray

For the Lagrangian model, since the space charge field is computed by accounting for the charge contribution of every droplet at its respective position, the accuracy of the field will be determined by how faithfully the simulated snapshot of the spray plume represents the observed behavior. Furthermore, in light of the discussion in the previous section, the model must account for the distribution of both primary and satellite droplets. Fig. 7 shows a comparison between a real spray image (right) and a snapshot of a half-plume (left) produced by the Lagrangian code described in Section 3.2.

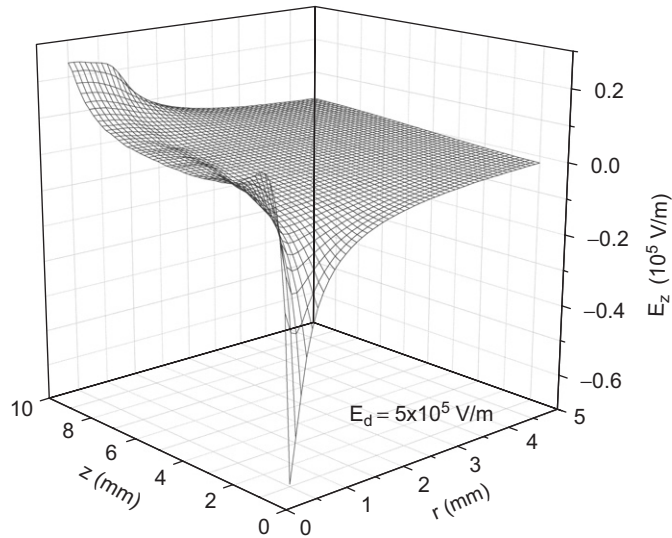


Fig. 8. Space charge field of a single electro spray computed by a Lagrangian model.

The model is able to capture the plume shape and the confinement of the satellite droplets to an outer shroud that is distinct from the spray core of primary droplets. Quantitatively, the code predicted that the minimum driving field to prevent satellite trapping is 8×10^4 V/m, which is only 7% larger than the experimental value of 7.5×10^4 V/m.

Fig. 8 shows the axial space charge field acquired by averaging 50 spray “snapshots” from the Lagrangian code. The field is most intense where the spray is not fully open, and an electrostatic “barrier” is formed within the first millimeter from the extractor, in which the space charge field is negative, pushing the droplets back toward the extractor. If the combination of droplet inertia and the electric driving force is large enough, the satellite droplet may overcome the trapping effect of the space charge and escape this critical zone.

For the line-of-charge model, the asymptotic form of equation (2) in the critical zone ($z \ll z_0$ and $r \ll z_0$) is

$$E_z = \frac{-\lambda}{2\pi\epsilon_0\sqrt{r^2 + z^2}}. \quad (13)$$

Eq. (13) also exhibits a steep slope near the origin, which is consistent with the axial component of the space charge field in Fig. 8.

Fig. 9 shows a comparison between the axial components of space charge fields E_z , as computed by the Lagrangian model and by the line-of-charge model, in several planes parallel to the extractor. Most of the E_z curves in Fig. 9 exhibit modest slopes except at $z = 0.2$ mm, where a steep change occurs within the “critical” zone. The line-of-charge model agrees with the Lagrangian model *outside* the spray. While inside the spray, in the region near the axis for $2 \text{ mm} < z < 4 \text{ mm}$, for instance, some discrepancy is expected and is irrelevant in the context of satellite trapping.

Fig. 10 shows the radial field component comparison between the Lagrangian model and the line-of-charge model, i.e. Eq. (3). The solid curves are $E_r(r, z_i)$ calculated using the Lagrangian model at 50 different z_i planes from 0 to 10 mm in 0.2 mm increments. As r increases, each $E_r(r, z_i)$ first starts to increase for positions inside the spray; it reaches a peak when r approaches the boundary of the spray and finally starts to decay outside the spray. The envelope formed by $E_r(r, z_i)$ of all z_i planes coincides with the line-of-charge approximation within 20%.

As discussed at the end of Section 3.1, Eq. (8) describes the trajectory of the outermost primary droplet, or the plume shape, and Eq. (9) describes the trajectory of a satellite droplet, or the shroud shape. The results computed by Eqs. (8), (9) and by Lagrangian model of a typical spray are compared in Fig. 11. Both shapes of the primary droplet plume and of the satellite shroud modeled with the simple line-of-charge are in satisfactory agreement with the full model, while the CPU time decreases from several hours to a fraction of 1 s on a personal computer with a single core 2.1 GHz AMD Athlon CPU and 2 GB memory. After the successful verification of the line-of-charge model, we shall now extend the model to multiplexed electro sprays.

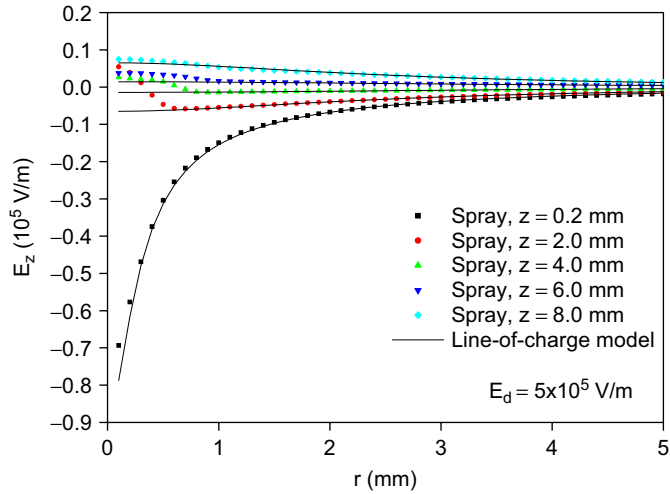


Fig. 9. Comparison of the Lagrangian model and the line-of-charge model: axial component of the space charge field in selected planes perpendicular to the electro spray axis.

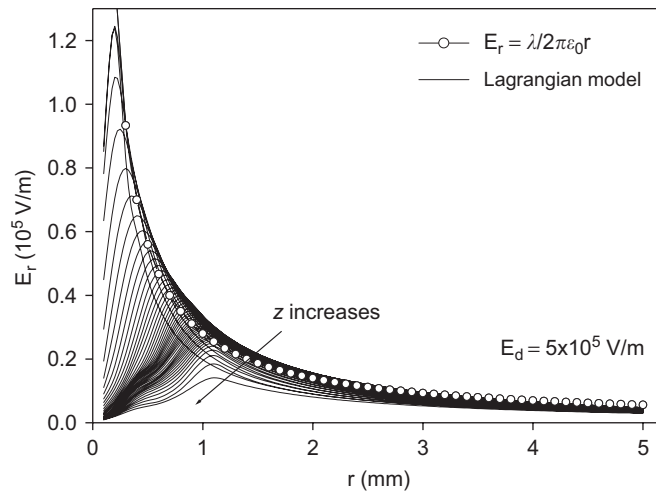


Fig. 10. Comparison of the Lagrangian model and the line-of-charge model: radial component of the space charge field.

5. The multiplexed electro spray modeled as multiple lines-of-charge

Implementing the multiple lines-of-charge model numerically is fairly straightforward: in addition to the single line-of-charge model at the center, multiple lines-of-charge were positioned in a hexagonal pattern, and the space charge field (E_r , E_z) was computed by summing up all the fields from each individual line-of-charge. Satellite trapping could be determined by tracking trajectories using Eq. (9).

To guide the expensive prototype microfabrication process, it is desirable to have an analytical, even if approximate, expression governing the limiting behavior of a multiplexed electro spray, in addition to the numerical model. The goal is to estimate the field in the critical zone where the satellite trapping is most likely to happen. In the case of multiplexed electro sprays this critical zone is around the center spray near the extractor, where the strongest axial component of the space charge field (E_z) appears. The radial component (E_r) in the critical zone is much less significant because its magnitude will be affected by partial cancellation from neighboring sprays on opposite sides. Furthermore,

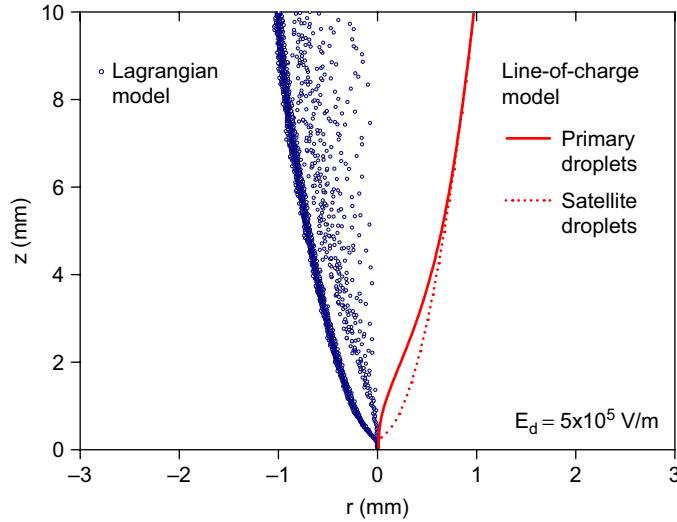


Fig. 11. Comparison of the Lagrangian model and the line-of-charge model: plume and shroud shape.

E_r does not directly contribute to the satellite trapping. Therefore, we shall focus on the analysis of E_z in the critical zone.

5.1. E_z in the critical zone

The geometry of the multiple lines-of-charge model is shown in Fig. 12. Each spray is assumed to be a line-of-charge of uniform intensity λ . The distance between two adjacent lines-of-charge is P , that is, the pitch of the nozzle array. E_z can be evaluated efficiently by grouping the sprays. The center spray is denoted as 0th group, the 1st group includes the six sprays that are at a distance P from the center, and the n th group has $6n$ sprays that are at a distance $\sim nP$ from the center (the actual distance ranges from $\sqrt{3}nP/2$ to nP). The z component of the electric field near the “critical zone” caused by the n th group is

$$E_{zn} = 6n \int_0^{z_0} \frac{\lambda z}{2\pi\epsilon_0((nP)^2 + z^2)^{3/2}} dz = \frac{-3n\lambda/\pi\epsilon_0}{\sqrt{(nP)^2 + z^2}} \Big|_0^{z_0} = E_{\text{ref}}(1 - (1 + (\alpha/n)^2)^{-1/2}), \quad (14)$$

where $E_{\text{ref}} = 3\lambda/(\pi\epsilon_0 P)$ and $\alpha = z_0/P$. For $(\alpha/n)^2 \gg 1$, $E_{zn} \rightarrow E_{\text{ref}}(1 - n/\alpha)$, and for $(\alpha/n)^2 \ll 1$, $E_{zn} \rightarrow E_{\text{ref}}(\alpha/n)^2/2$. Using the approximation $E_{zn} \approx E_{\text{ref}}(1 - n/\alpha)$ for $1 \leq n < \alpha$, and $E_{zn} \approx E_{\text{ref}}(\alpha/n)^2/2$ for $n \geq \alpha$, we find:

$$\sum_{n=1}^{\alpha-1} E_{zn}/E_{\text{ref}} \approx \sum_{n=1}^{\alpha-1} (1 - n/\alpha) \approx \alpha/2, \quad (15)$$

$$\sum_{n=\alpha}^{\infty} E_{zn}/E_{\text{ref}} \approx \sum_{n=\alpha}^{\infty} (\alpha/n)^2/2 \approx \alpha/2, \quad (16)$$

$$E_{\infty}/E_{\text{ref}} = \sum_{n=1}^{\infty} E_{zn}/E_{\text{ref}} \approx \alpha. \quad (17)$$

Eqs. (15)–(17) suggest that for a system with infinite number of sprays, half of the axial field is contributed by the sprays located within a radius $\sim z_0$ from the center spray, where z_0 is the distance between extractor and collector electrodes, and the other half is from the rest.

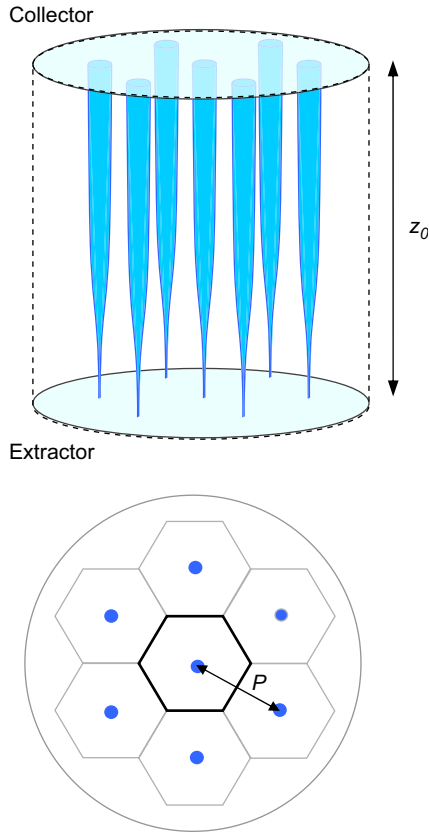


Fig. 12. Schematic of the geometry of the multiple lines-of-charge model.

5.2. Infinite multiplexing

Substituting $\lambda = I/v_z$ and $A = \sqrt{3}P^2/2$, the average area per nozzle in the hexagonal pattern of Fig. 12, in E_{ref} yields

$$E_{\text{ref}} = \frac{3\sqrt{3}}{2\pi\epsilon_0 v_z} \left(\frac{I}{A}\right) P. \tag{18}$$

Combining Eqs. (17) and (18) for a system with an infinite number of lines-of-charge yields

$$E_{\infty} = C_{\infty} t_r (I/A), \tag{19}$$

where $C_{\infty} = 3\sqrt{3}/2\pi\epsilon_0 = 0.827/\epsilon_0$, and t_r is the primary droplet residence time within the plume ($t_r = z_0/v_z \sim 1$ ms). The stopping time for the satellite droplet (τ_s) is estimated at 0.025 ms, which is much shorter than the primary droplet residence time (~ 1 ms). During τ_s the satellite displacement is ~ 0.2 mm, which is still within the 1 mm critical zone. Therefore, it appears that the satellite will lose momentum completely inside the critical zone if no other force is provided. To prevent satellite trapping, the net force toward the collector, for example, must be such that $E_d > E_{\infty}$, or,

$$E_d > C_{\infty} t_r (I/A). \tag{20}$$

Inequality (20) can serve as a design criterion for an infinitely multiplexed system imposing restrictions on the combination of the three parameters: E_d , t_r , and the current emitted per unit area. Since the current is a monotonic function of the flow rate, inequality (20) can also be used to estimate the maximum flow rate per unit area that can be dispersed for any predetermined E_d and t_r .

Table 1

Minimum driving field, E_d , to prevent satellite trapping for a system with n “rings” of nozzles: comparison between experiments and models for different degrees of multiplexing ($\alpha = 14.8$, $z_0 = 10$ mm, $P = 0.675$ mm, flow rate per nozzle at 0.6 cc/h)

Number of rings	0	1	2	5	10	∞
Number of nozzles	1	7	19	91	331	∞
E_d , experiment (10^5 V/m)	0.75	2.3	3.4	6.5	11.0	N/A
E_d , numerical multiple lines-of-charge (10^5 V/m)	0.71	2.1	3.6	7.6	12.6	N/A
E_d , analytical multiple lines-of-charge (10^5 V/m)	0.80	2.8	4.6	9.2	14.2	31.7

Table 2

Effect of the electrode aspect ratio, α , on the minimum driving field to prevent satellite trapping, E_d , comparison between experiments and models for different P (19 nozzles, $z_0 = 10$ mm, flow rate per nozzle at 0.6 cc/h)

α	14.8	7.4
E_d , experiment (10^5 V/m)	3.4	2.3
E_d , numerical multiple lines-of-charge model (10^5 V/m)	3.6	1.9
E_d , analytical multiple lines-of-charge (10^5 V/m)	4.6	2.7

Now we will compare Eq. (19) with the following even simpler model. If we treat the infinite domain boundaries as two parallel electrodes and assume a uniform volume charge density, ρ_s , throughout the calculation domain, one can easily derive from Poisson’s equation that the space charge field is linear, and the strongest value $E_s = \pm \rho_s z_0 / (2\epsilon_0)$ appears at the boundaries. Since $\rho_s = I / (Av_z)$,

$$E_s = C_s \tau (I/A), \quad (21)$$

where $C_s = 1 / (2\epsilon_0) = 0.5 / \epsilon_0$. Eqs. (19) and (21) have similar forms, which is another verification of the model. The constant C_∞ is larger than C_s by 65% because the uniform space charge assumption evens out the steep critical zone caused by the jet when it has not opened up fully into a spray yet.

5.3. Finitely multiplexed system

For a finite system with n “rings” of nozzles ($n < \alpha$), the space charge field caused by all nozzles is

$$E_{\text{sum}} = \sum_{k=1}^n E_{zn} \approx E_{\text{ref}} \sum_{k=1}^n (1 - k/\alpha) = E_\infty [n/\alpha - (n+1)n/2\alpha^2]. \quad (22)$$

The estimate of the necessary driving field to prevent satellite trapping for such a system yields

$$E_d > E_{z0} + E_{\text{sum}} = E_{z0} + C_\infty \tau (I/A) [n/\alpha - (n+1)n/2\alpha^2], \quad (23)$$

where E_{z0} is the minimum field to eliminate satellite trapping for the single spray. A comparison of the estimated driving field E_d between the analytical model, the numerical model, and the experimental values is shown in Table 1. The data show that the numerical multiple lines-of-charge model agrees with the experiment within 17%, while the analytical estimate has a larger discrepancy of up to 42%. The analytical estimates are always larger than experimental values for the following reasons: (a) the analytical solution is a conservative estimate since the satellite inertia is neglected; (b) the primary droplets may be accelerated by the external field and the effective λ would decrease as compared to the originally estimated λ that was based on the initial jet velocity; (c) the sprays repel each other further downstream, so the volume charge density decreases and the space charge field is weakened.

Inequality (23) suggests that, if the residence time and the current emitted per unit area are fixed, E_d will decrease with α , which could be realized by increasing P . To check this behavior, a 19-nozzle array with a $2P$ pitch was prepared by clogging every other ring of nozzles in a 91-nozzle wafer. The experimental and modeled fields showed that indeed the space charge is significantly weaker when the aspect ratio α is decreased by 50%, as shown in Table 2.

Inequality (23) also implies that the current emitted per unit area has a strong effect on the field. To verify this effect experimentally, we enhanced the liquid conductivity by doping the pure ethanol with 5 ppm (by weight) of an ionic

Table 3

Minimum driving field, E_d , to prevent satellite trapping for a system with n “rings” of nozzles and inter-nozzle pitch, P : comparison between experiments and models at “high” current (ethanol + 5 ppm IL, $K = 1.0 \times 10^{-4}$ S/m, flow rate per nozzle at 0.6 cc/h)

	1 ($P = 0.675$ mm)	2 ($P = 0.675$ mm)	2 ($P = 1.35$ mm)
Number of rings	1	2	2
Number of nozzles	7	19	19
E_d , experiment (10^5 V/m)	6.0	9.0	5.1
E_d , analytical multiple lines-of-charge (10^5 V/m)	7.0	10.8	6.4

liquid (1-ethyl-3-methylimidazolium ethylsulfate). Consequently, at the same flow rate, the current emitted from each nozzle was increased from 10 to 39 nA. Table 3 summarizes the test results. Compared to the pure ethanol, the doped ethanol needs considerably stronger driving field to prevent satellite trapping. The model predicted the driving field with acceptable accuracy.

6. Conclusion

An investigation was conducted on the limitations to electrospray multiplexing brought about by space charge. Experimentally, it was observed that with an increase in flow rate, conductivity, and/or multiplexing density, conditions are reached when satellite droplets in the electrospray reverse their path, impacting on the extractor electrode, flooding it and eventually shorting out the electric field between the extractor electrode and the spray nozzles.

The space charge field of a single electrospray was numerically investigated using a Lagrangian model which accounted for the contribution to the field from every droplet. The morphology of the computed spray pattern, from the plume of primary droplets to the shroud of satellite droplets, was found to be in good agreement with two-dimensional images of the spray under laser-sheet illumination. The analysis was simplified by approximating the presence of the spray of charged droplets with a line-of-charge, which correctly reproduced the spray shape and the electric field *outside* the spray.

The latter feature is particularly useful to model space charge effects in multiplexed electrosprays since the mutual influence of a spray on its neighbors is affected by the space charge field outside the spray. As a result, the electric interaction of multiplexed electrosprays can be modeled using a multiple lines-of-charge model, with a dramatic reduction in computational time, as compared to the full Lagrangian model. Additional analytical approximations of this simplified model yielded a scaling law, showing the dependence of the space charge on: (i) the primary droplet residence time, (ii) the current emitted per unit area, and (iii) the dimensionless parameter, α , that is the ratio of z_0 , the distance between the extractor and the ground electrode, to P , the distance between two neighboring nozzles. Experimental data confirmed that the model estimates the space charge field reliably and provides design guidelines for large-scale electrospray multiplexing, without the need of costly, trial-and-error prototyping by microfabrication.

Acknowledgments

The authors would like to thank Mr. Chris M. Waits and Mr. Nick Jankowski who were responsible for the microfabrication in the U.S. Army Research Laboratory, and Prof. Juan Fernández de la Mora for valuable suggestions. The support of the U.S. Army under Grant no. W911NF-05-2-0015 (Mr. Bruce Geil, Contract Monitor) is gratefully acknowledged.

References

- Bocanegra, R., Galán, D., Márquez, M., Loscertales, I. G., & Barrero, A. (2006). Multiple electrosprays emitted from an array of holes. *Journal of Aerosol Science*, 36, 1387–1399.
- Chen, D., & Pui, D. Y. H. (1997). Experimental investigation of scaling laws for electrospraying: Dielectric constant effect. *Aerosol Science and Technology*, 27(3), 367–380.
- Cloupeau, M., & Prunet-Foch, B. (1989). Electrostatic spraying of liquids in cone-jet mode. *Journal of Electrostatics*, 22(2), 135–159.
- COMSOL Group (2007). (<http://www.comsol.com/>).
- De Juan, L., & Fernández de la Mora, J. (1997). Charge and size distribution of electrospray drops. *Journal of Colloid Interface Science*, 186, 280–293.

- Deng, W., Klemic, J. F., Li, X., Reed, M., & Gomez, A. (2006). Increase of electrospray throughput using multiplexed microfabricated sources for the scalable generation of monodisperse droplets. *Journal of Aerosol Science*, 37, 696–714.
- Deng, W., Klemic, J. F., Li, X., Reed, M., & Gomez, A. (2007). Liquid fuel combustor miniaturization via microfabrication. *Proceedings of the Combustion Institute*, 31, 2239–2246.
- Fenn, J. B., Mann, M., Meng, C. K., Wong, S. F., & Whitehouse, C. M. (1989). Electrospray ionization for mass spectrometry of large biomolecules. *Science*, 246(4926), 64–71.
- Fernández de la Mora, J. (1992). The effect of charge emission from electrified liquid cones. *Journal of Fluid Mechanics*, 243, 561–574.
- Frenkel, D., & Smit, B. (2002). *Understanding molecular simulation: From algorithms to applications*. (2nd ed.), Anonymous London, UK: Academic Press.
- Ganan-Calvo, A. M., Lasheras, J. C., Davila, J., & Barrero, A. (1994). Electrostatic spray emitted from an electrified conical meniscus. *Journal of Aerosol Science*, 25, 1121–1142.
- Gomez, A., Bingham, D., De Juan, L., & Tang, K. (1998). Production of protein nanoparticles by electrospray drying. *Journal of Aerosol Science*, 29(5–6), 561–574.
- Li, K.-Y., Tu, H., & Ray, A. K. (2005). Charge limits on droplets during evaporation. *Langmuir*, 21, 3786–3794.
- Lozano, P. (2003) *Studies on the ion-droplet mixed regime in colloid thrusters*. Thesis, MIT.
- Rosell-Llompart, J., & Fernandez de la Mora, J. (1994). Generation of monodisperse droplets 0.3 to 4 μm in diameter from electrified cone-jets of highly conducting and viscous liquids. *Journal of Aerosol Science*, 25, 1093–1119.
- Sakiadis, B. C. (1961). Boundary-layer behavior on continuous solid surfaces: III. The boundary layer on a continuous cylindrical surface. *A.I.Ch.E. Journal*, 7, 467–472.
- Tang, K., & Gomez, A. (1994). On the structure of an electrostatic spray of monodisperse droplets. *Physics of Fluids*, 6, 2317–2332.
- Tang, K., Lin, Y., Matson, D. W., Kim, T., & Smith, R. D. (2001). Generation of multiple electrosprays using microfabricated emitter arrays for improved mass spectrometric sensitivity. *Analytical Chemistry*, 73(8), 1658–1663.
- Velásquez-García, L. F., Akinwande, A. I., & Martínez-Sánchez, M. (2006). A planar array of micro-fabricated electrospray emitters for thruster applications. *Journal of Microelectromechanical Systems*, 15, 1272–1280.
- Wilhelm, O., Mädler, L., & Pratsinis, S. E. (2003). Electrospray evaporation and deposition. *Journal of Aerosol Science*, 34, 815–836.